ID Design Press, Skopje, Republic of Macedonia
Open Access Macedonian Journal of Medical Sciences. 2019 Dec 15; 7(23):4101-4109.
https://doi.org/10.3889/oamjms.2019.868
eISSN: 1857-9655
***Dental Sciences***

# Effect of Sofosbuvir Administration and Its Withdrawal on the Submandibular Salivary Gland of Adult Male Albino Rats: A Histological and Ultra-Structural Study

Asmaa Mahmoud Abdeen[1*], Tarik Essawy[2], Saher Sayed Mohammed[1]

*[1]Oral Biology Department, Faculty of Dentistry, MINIA University, Minia, Egypt; [2]Oral Biology Department, Faculty of Dentistry, Cairo University, Cairo, Egypt*

**Citation:** Abdeen AM, Essawy T, Mohammed SS. Effect of Sofosbuvir Administration and Its Withdrawal on the Submandibular Salivary Gland of Adult Male Albino Rats: A Histological and Ultra-Structural Study. Open Access Maced J Med Sci. 2019 Dec 15; 7(23):4101-4109. https://doi.org/10.3889/oamjms.2019.868

**Keywords:** Sofosbuvir; Submandibular salivary gland; Histological study; Ultra-structural study

***Correspondence:** Asmaa Mahmoud Abdeen. Oral Biology Department, Faculty of Dentistry, Minia University, Minia, Egypt. E-mail: asmaa.3abdeen@mu.edu.eg

**Received:** 08-Oct-2019; **Revised:** 24-Nov-2019; **Accepted:** 25-Nov-2019; **Online first:** 10-Dec-2019



**Funding:** This research did not receive any financial support

**Competing Interests:** The authors have declared that no competing interests exist

**Abstract**

**BACKGROUND:** Sofosbuvir (SOF) was approved in 2013 as a part of first-line treatment for hepatitis C virus (HCV); it has activity against all genotypes with extrahepatic adverse effects have recently arisen.

**AIM:** Investigating sofosbuvir-induced alterations in the rat submandibular salivary gland (SMSG).

**METHODS:** A group of 80 adult albino rats weighing about ± 150 gm were used in the experiment. The rats were divided into 3 groups: Group I (control group) received distilled water, Group II (experimental group) divided into 2 subgroups and received SOF 40 mg/kg/day dissolved in distilled water for 1 and 3 months and Group III (recovery group) allowed for 1 month of recovery after SOF withdrawal. All animals were sacrificed; the SMSG was dissected, and specimens were examined histologically and ultra-structurally.

**RESULTS:** Compared to Group I, Group II subgroup (1) showed acinar and ductal vacuolisation, discontinuity of the epithelial lining associated with retained secretion and congested blood vessels. These changes were found to be exaggerated in the subgroup (2) accompanied by acinar and ductal shrinkage, interstitial oedema, haemorrhage, chronic inflammatory cells infiltration and loss of gland compactness. Amelioration of the histological changes was detected in Group III after SOF withdrawal. The ultrastructural examination confirmed these histological results.

**CONCLUSION:** SOF had induced apparent alterations in the structure and ultrastructure of SMSG. The SOF-induced alterations were time-dependent, attributed mainly to mitochondrial toxicity and partially ameliorated by its withdrawal.

## Introduction

Hepatitis (C) is an infectious disease that affects the liver and is caused by the hepatitis C virus (HCV). An estimated 130-200 million people worldwide are infected with HCV (Ryan and Ray, 2004) [20].

Hepatitis (C) anti-viral therapy has undergone a revolution, moving very rapidly from IFN-based therapies with the sustained virological response (SVR) of 40–70%, to the advent of direct-acting antiviral drugs (DAAs) achieving (SVR) over 90% for all genotypes (Thomas, 2010) [31].

There is a new generation of DAAs, which included sofosbuvir (SOF), simeprevir (SIM) and daclatasvir (DCV). These drugs exhibited high efficacy, wide therapeutic index and great difficulty for resistance development for patients with prior DAAs treatment failure (Sene et al., 2004) [24].

Sofosbuvir was a nucleotide analogue which was approved by the United States Food and Drug Administration (FDA) in 2013; it is administered once-daily as a 400 mg oral tablet for just 12 weeks with the same in vitro activity against all HCV genotypes (Jacobson et al., 2013 [13].

Sofosbuvir is converted to its active metabolite directly at the liver by enzymes located in the human hepatic cells. The active nucleotide form (GS- 461203) is metabolised to the inactive metabolite of the nucleotide, (GS-331007). This metabolite is largely eliminated by passive filtration in the renal

glomerulus, and it mimics the physiological nucleotide. It competitively blocks the NS5B polymerase, which is the viral RNA polymerase, thus inhibiting the HCV-RNA synthesis by RNA chain termination (Zeng et al., 2013 [32]; Soriano et al., 2013 [27]).

Before the discovery of SOF, different nucleotide analogue inhibitors (NIs) have been tested as anti-hepatitis C treatments. Infrequent but serious adverse events have been reported with these oral (NIs). All nucleotide analogues have a “black box warning” regarding potential mitochondrial toxicity in their product labelling (Johnson et al., 2001) [14].

From the above review, it seems that SOF is a promising therapy for chronic HCV infection; however, its adverse effects on oral tissues in specific as one of (NIs) had not been well documented. Thus, the present study aimed to investigate the possible effect of SOF on the SMSG of adult albino rats, histologically and ultra-structurally.

## Material and Methods

Animals: 80 adult male albino rats were used in this experiment; each was 5-6 weeks old and weighed 100-150 grams. They were fed on standard chow pellets and tap water ad libitum to adjust to the laboratory conditions 1 week before the experiment and for the entire experiment period, in the faculty of Medicine, Minia University in Egypt. All aspects of animal care and treatment were carried out by the research protocols established by Institute of Laboratory Animal Research, 1996 and in accordance to the recommendations and approval of the Ethics Committee on Animal Experimentation of the Faculty of Dentistry, Minia University in Egypt.

Sofosbuvir (SOF) preparation: SOF was a product of Pharco Pharmaceuticals, Alexandria, Egypt; it was available in the form of tablets with the trade name ‘Gratisovir’. Animals have received the acceptable daily dose of SOF dissolved in distilled water (4 mg/ml) through oral gavage in a dose equivalent to 40 mg/kg body weight (Shin et al., 2010) [25].

Experimental design: The animals were divided into three groups:

Group I (Control): composed of 20 rats were received an ordinary rat diet and distilled water through oral gavage.

Group II (experimental group): composed of 40 rats were divided into:

Subgroup (1): 20 rats were given 40 mg/kg body weight of SOF daily for 1 month.

Subgroup (2): 20 rats were given 40 mg/kg body weight of SOF daily for 3 months.

Group III (recovery group): composed of 20 rats. They have received the dose above of SOF for 3 months; after that, they were left untreated for one month.

At the end of the dedicated duration for each, all rats were anaesthetised with an intraperitoneal injection of sodium pentobarbital (50 mg/kg) (Fish, Danneman, Brown, & Karas, 2011) [9]. The skin of the neck was incised, and the SMSGs were dissected out. Specimens from both glands were preserved in the fixatives and processed for:

Light microscopic examination: Specimens were immediately fixed in 10% neutral formalin for 48 h, washed, dehydrated in ascending grades of alcohol, embedded in paraffin and sectioned at (4-5 µm) in thickness. They were conventionally stained with Haematoxylin and Eosin. Sections were examined and photographed using Biological Light Microscope (LEICA, DM LB100T, Germany) fitted with a digital camera (LEICA Microsystem, DFC295, Germany), at the Histopathological Unit, Minia University.

Electron microscope examination: 4 blocks (1 x 2 mm) were taken from each sample and Fixed in 5 % cold glutaraldehyde immediately after dissection of the SMSG for 24 – 48 h. The specimens were then washed in cacodylate buffer (PH 7.2) 3 – 4 times for 20 minutes every time and postfixed in 1% O4 s4 for 2 hours, after that washed in the same buffer 4 times. Dehydration by ascending grades of alcohol (30 – 50 – 70 – 90 and 100% 2 hours) of each was done and was embedded in epon – araldite mixture according to the protocol of Electron Microscope Unit, Assiut University, Egypt. From the embedded blocks semi-thin sections by L KB ultra-microtome in the thickness of (0.5 – 1 m) were prepared for orientation of the tissue and photographed by sc30 Olympus camera and then ultrathin section in thickness of (500 – 700 A) were made using Leica AG ultra-microtome and contrasted in uranyl acetate and lead citrate. Sections were examined by JEM 100 CXII Electron Microscope (EM) at 80 KV and photographed by CCD digital camera Model XR-41 at the Electron Microscope Unit, Assiut University.

## Results

### *Light Microscope Results*

Group I (The Control Group): The SMSG showed normal architecture consisting of secretory end pieces; collecting ducts and granular convoluted tubules (GCTs) invested in a reticular connective tissue (C.T.) stroma containing blood vessels (Fig. 1).

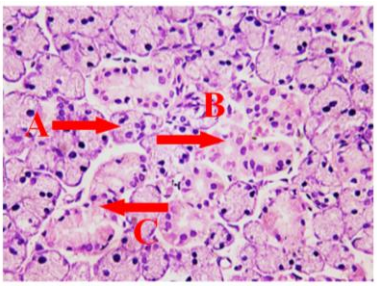


*Figure 1: A photomicrograph of rat SMSG of group I (control group) showing normal histological structure: A) Serous acini; B) striated duct, and C- GCTs (H & E, X 400)*

*Group II (The Experimental Group):*

Subgroup 1:

Specimens of this experimental subgroup showed that most acini appeared with obvious micro and macro-vacuolization; some acini showed ill-defined boundaries and were slightly distended (Fig. 3). The nuclei exhibited numerous mitotic figures, including normal and abnormal mitosis (Fig. 2).

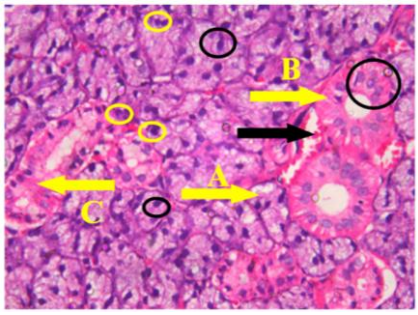


*Figure 2: A photomicrograph of group II (experimental group) subgroup 1 showing: A- serous acini with micro-vacuoles, B- striated duct with peripheral nuclear proliferation and surrounding congested blood vessels (black arrow), C- GCT with stagnated eosinophilic coagulum and D- some nuclei with normal mitosis (yellow circles) and others with abnormal mitosis (black circles) (H & E, X 400)*

Striated ducts showed peripheral areas of nuclear proliferation and GCTs showed retained eosinophilic coagulum in their lumen (Fig. 2).

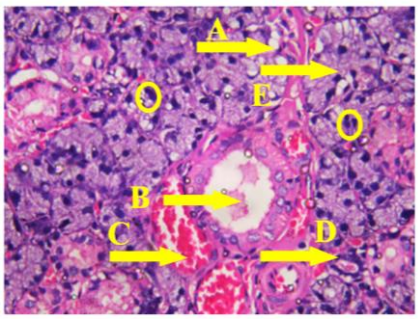


*Figure 3: A photomicrograph of group II (experimental group) subgroup 1 showing: A- acini with macro-vacuoles, abnormal mitosis (yellow circles), B- excretory duct with stagnant secretion, C- engorged blood vessel with collected R.B.Cs, D- mild blood hemorrhage, E- distended serous acini (H & E, X 400)*

Excretory ducts appeared with some stagnant secretion. The blood vessels were slightly dilated, engorged with RBCs with speckled area of hemorrhage (Fig. 3). Intra-lobular fat cells infiltration was recognised (Fig. 8).

Subgroup 2:

Specimens of this experimental subgroup showed most aggravated changes with complete loss of normal glandular morphological pattern and increase of interstitial oedema. The acini exhibited massive atrophic changes, disrupted boundaries, vacuolar degeneration, faintly stained cytoplasm and pyknotic nuclei (Fig. 4).

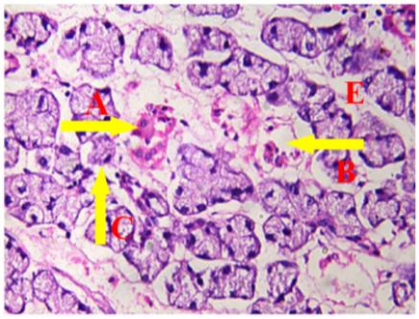


*Figure 4: A photomicrograph of group II (experimental group) subgroup 2 showing: A-degenerated striated duct with atrophied epithelial lining and macro-vacuoles, B- complete degenerated GCTs with epithelial remnants and pyknotic nuclei, C- shrinked serous acini with un defined outlines, and (E) widened intercellular spaces (H & E, X 400)*

The striated ducts and GCTs showed indistinguishable boundaries, thinning of the epithelial lining, total loss of cytoplasmic content and pyknotic nuclei. Some ducts presented as (Ghost shape) with only remnants of ducts were found (Fig. 4). Excretory duct showed thin and vacuolated epithelial lining associated with wide lumen filled with epithelial remnants and cellular debris. Blood vessels appeared thin and dilated with extravasated RBCS (Fig. 5).

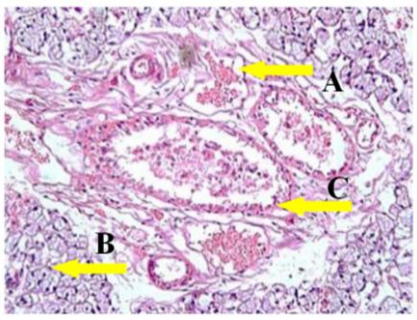


*Figure 5: A photomicrograph of group II (experimental group) subgroup 2 showing: A- congested B.V., B- shrinked serous acini, C- thin and vacuolated epithelial lining of excretory duct associated with wide lumen filled with cellular debris (H & E, X 400)*

Extensive fat cells were noticed in the C.T. stroma (Fig. 8).

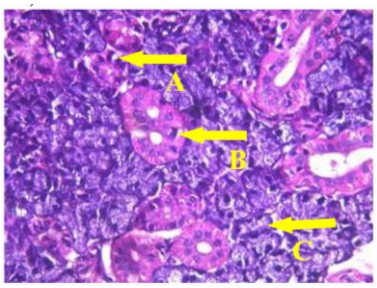


*Figure 6: A photomicrograph of group III (recovery group) showing: A-cross section of GCT with microvacuolation and hyperchromatic nuclei, B- striated duct with hyperchromatic nuclei and microvacuoles, C- shrinked serous acini with surrounding interacinar oedema (H & E, X 400)*

*Group III (The Recovery Group):*

Specimens of this group showed amelioration of the structural changes induced by SOF, intralobular acini and ducts were more or less as a control group associated with hyperchromatic nuclei and peripheral areas of proliferation.

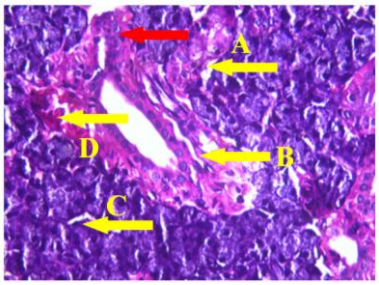


*Figure 7: A photomicrograph of group III (recovery group) showing: A- GCT with deeply stained coagulum and surrounding oedema, B- excretory duct with slightly recovered epithelium, hyperchromatic nuclei and peripheral area of proliferation (red arrow), C- interacinar oedema, D- slightly congested B.V. (H & E, X 400)*

Nevertheless, cytoplasmic vacuolisation were detected with slight interstitial oedema (Fig. 6). Blood vessels showed a minimal amount of congestion (Fig. 7) and massive fatty cells infiltration was persistent (Fig. 8).

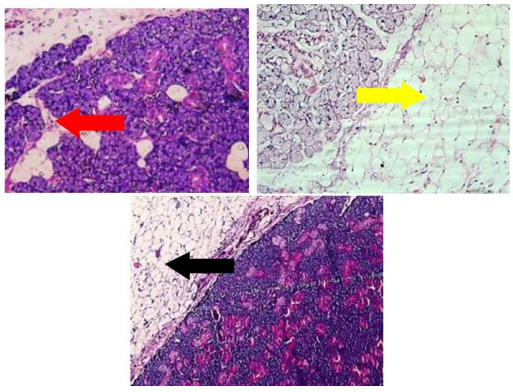

*Figure 8: A photomicrograph of group II (experimental group) and group III (recovery group) showing: extensive fat cells infiltration began as intra-lobular infiltration (red arrow) in experimental subgroup (1) then increased gradually on the outer C.T. capsule in experimental subgroup (2) (yellow arrow) and persist in recovery group (black arrow) (H & E, X 200)*

***Transmission Electron Microscope Results***

*Group I (The Control Group):*

Examination of ultrathin sections revealed normal ultrastructure of the gland. The serous acini surrounded with very thin interacinar stroma and the acinar cells appeared to be filled with electron-lucent zymogen granules and contained basally situated vesicular nuclei (Fig. 9).

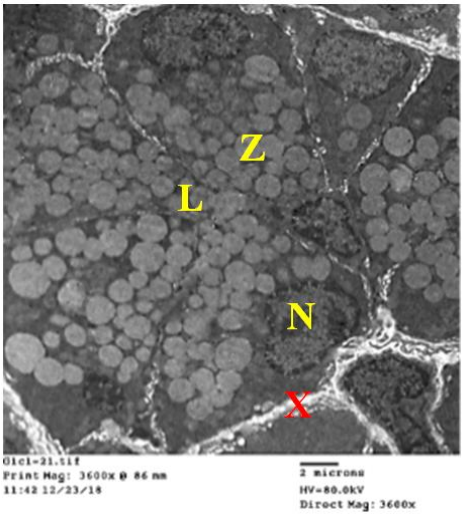


*Figure 9: T.E. micrograph of serous acini of control group displayed: basally situated vesicular nucleus (N), electron-lucent zymogen granules (Z), narrow lumen (L) and thin interacinar stroma (X) (TEM ×3600)*

Striated duct lining exhibited large vesicular rounded nucleus and numerous mitochondria incorporated within the basal cell membrane infoldings in addition to the presence of small electron-dense granules and short microvilli in their luminal cytoplasm surrounding wide lumen filled with secretion (Fig. 10).

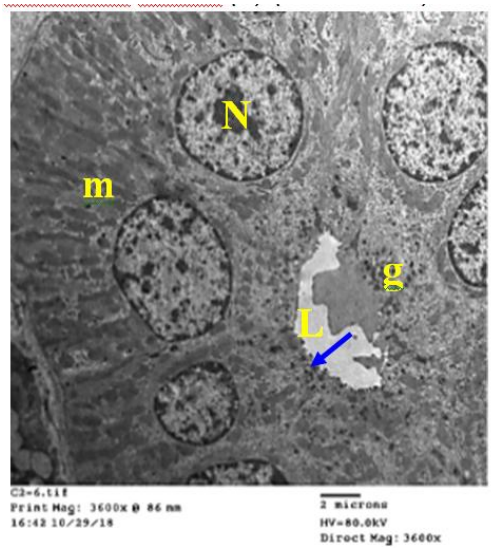


*Figure 10: T.E. micrograph of striated duct of control group displayed: elongated epithelial lining with large vesicular nucleus (N), regularly oriented mitochondria (m), small electron-dense granules (g) and short microvilli (arrow) surrounding wide lumen filled with secretion (L) (TEM ×3600)*

*Group II (The Experimental Group):*

Subgroup 1:

Examination of ultrathin sections of this subgroup showed the serous acinar cells presented with indented vesicular nuclei with different mitotic figures surrounded with small amount of cytoplasm. The intercellular connections were mostly separated duo to the presence of macro-vacuoles associated with undefined outlines. The secretory granules appeared larger, over accumulated, and some of them appeared to be coalesced to each other (Fig. 11).

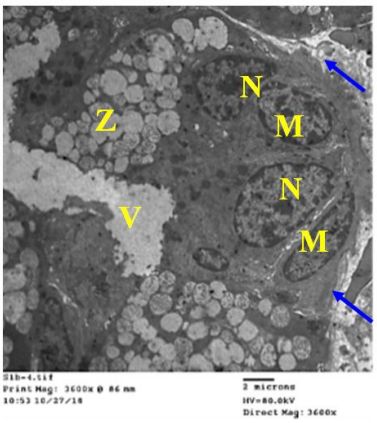


*Figure 11: T.E. micrograph of serous acini of experimental subgroup (1) displayed: accumulated electron-lucent zymogen granules (Z) some were coalesced to each other, large vesicular nucleus (N) with abnormal mitosis (M) and intercellular connections separated with macro-vacuoles (v) and undefined outlines (arrows) (TEM ×3600)*

Striated duct appeared more or less with normal morphology; it showed apparent striation rich in mitochondria, indented pleomorphic nuclei with some appeared to be hyperchromatic, and others appeared to be shrunk and the cytoplasm showed normal criteria. Widening of the interstitial spaces was noticed (Fig. 12).

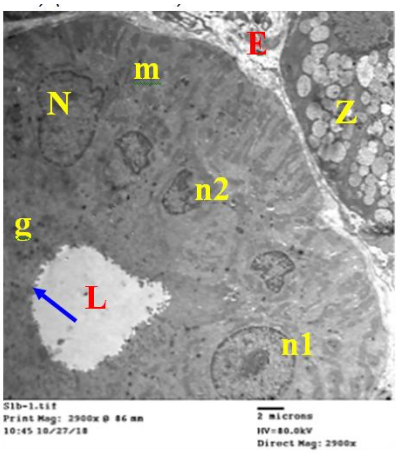


*Figure 12: T.E. micrograph of striated duct of experimental subgroup (1) displayed: columnar cells with indented pleomorphic nuclei (N) some were hyperchromatic (n1) and others were shrinked (n2), apical small electron-dense granules (g), microvilli in the luminal surface of the cells (arrow), basal striation with normal mitochondrial orientation (m), slight oedema (E) in the interstitial tissue and zymogen granules of the neighboring serous acini (Z) (TEM ×2900)*

Subgroup 2:

Examination of ultrathin sections of this subgroup showed severe necrobiotic changes. Serous acinar cells showed signs of degeneration in the form of pyknotic heterochromatic nuclei, widened intercellular spaces with undetected intercellular junctions, fatty cells infiltration and overloaded fused secretory granules forming little lakes. The lumen was nearly obliterated with accumulated electron-dense debris (Fig. 13).

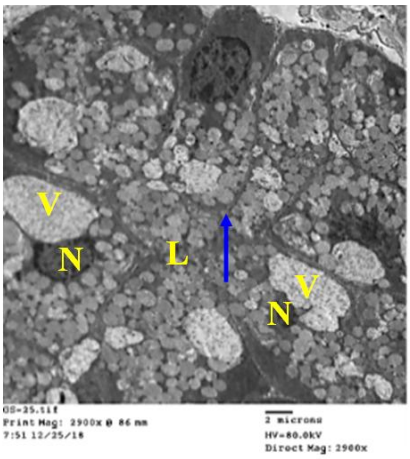


*Figure 13: T.E. micrograph of serous acini of experimental subgroup (2) displayed: shrinked acini with overloaded zymogen granules coalesced to each other forming lakes like vacuoles (V), pyknotic nuclei (N), widened intercellular spaces with undetected intercellular junctions (blue arrow) and obliterated lumen (L) (TEM ×2900)*

Striated duct showed vacuolated and disfigured epithelial lining with ill-defined outlines, obliterated lumen and complete loss of basal striation. Cells showed karyolitic nuclei, fragmented and swollen RER and mitochondria with variable grades of affection ranging from swelling and losing of their normal orientation up to losing of cristae and even complete cristolysis (Fig. 14).

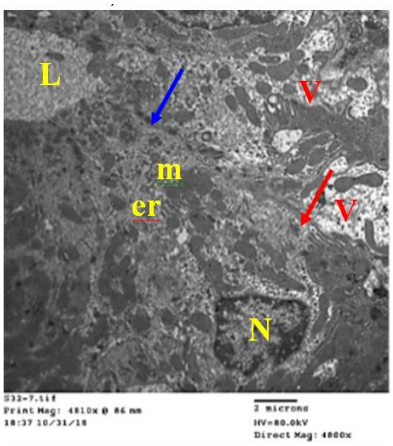


*Figure 14: T.E. micrograph of striated duct of experimental subgroup (2) displayed: marked vacuolation of the epithelial lining (V), loss of basal striation (red arrow), loss of intercellular junctions (blue arrow), karyolitic nuclei (N), degenerated swollen mitochondria (m), dilated fragmented RER (er) and obliterated lumen (L) (TEM ×4800)*

Interstitial tissues appeared to show severe oedema and inflammatory cells infiltration mostly of macrophage and eosinophil cells; the late appeared to contain a large number of elliptical granules and lobulated nucleus (Fig. 15).

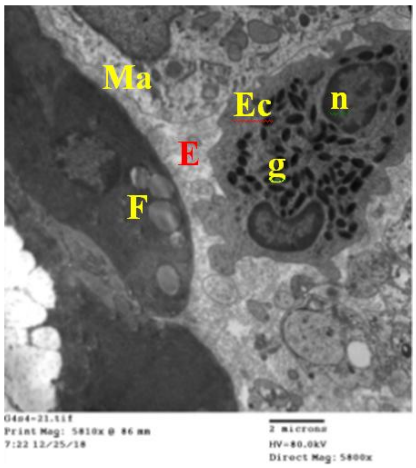


*Figure 15: T.E. micrograph of interstitial stroma of experimental subgroup (2) displayed: Eosinophil cell (Ec) contained large amount of elliptical granules (g) and lobulated nucleus (n), macrophage (Ma), fatty degeneration of serous acini (F) and severe oedema (E) (TEM ×5800)*

*Group III (The Recovery Group):*

Recovery group ultrathin sections revealed partial amelioration of the changes induced by SOF. Serous acinar cells showed large coalescent electron-lucent granules compressing the indented vesicular nuclei, which presented different mitotic figures and peripheral clumping of chromatin. The abundance of myoepithelial cells enclosing the acini were noticed with fatty droplets infiltration and mild interacinar oedema (Fig. 16).

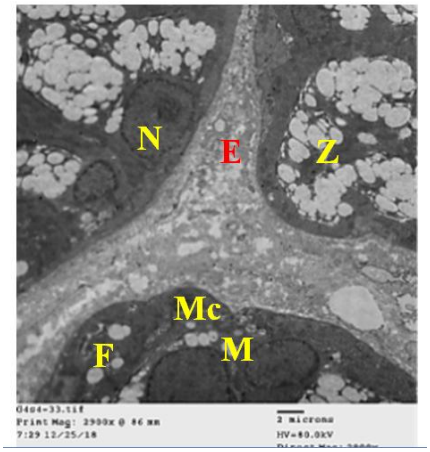


*Figure 16: T.E. micrograph of serous acini of recovery group displayed: numerous mitotic figures (M), basally situated vesicular nucleus (N), large amount of polymorph zymogen granules (Z), flat myoepithelial cells (Mc) enclosing the acini with pronounced fatty droplets infiltration (F) and interstitial oedema (E) (TEM ×2900)*

Striated ducts displayed columnar cells with large vesicular euchromatic nuclei, wide lumen and basal membrane infoldings with uniform mitochondrial orientation (Fig. 17).

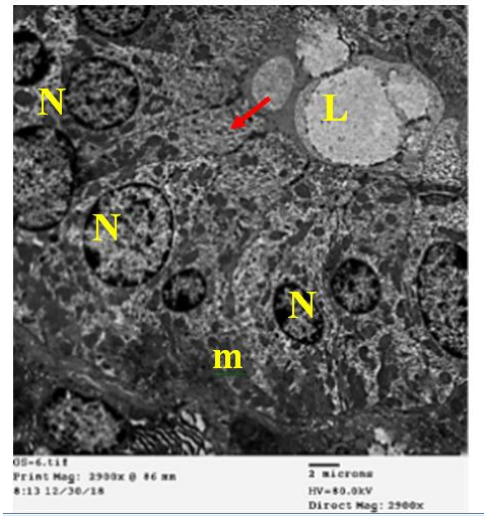


*Figure 17: T.E. micrograph of striated duct of recovery group displayed: well-defined columnar cells with vesicular nucleus (N) showing different mitotic figures, basal striation containing uniformly oriented mitochondria (m), reconnected intercellular junctions (arrow) and wide lumen (L) (TEM ×2900)*

Peculiar to this group presence of cellular infiltration, mostly plasma cells contained a large amount of cystic dilated RER (Russel bodies) were detected with mild interstitial oedema and dilated blood vessels (Fig. 18).

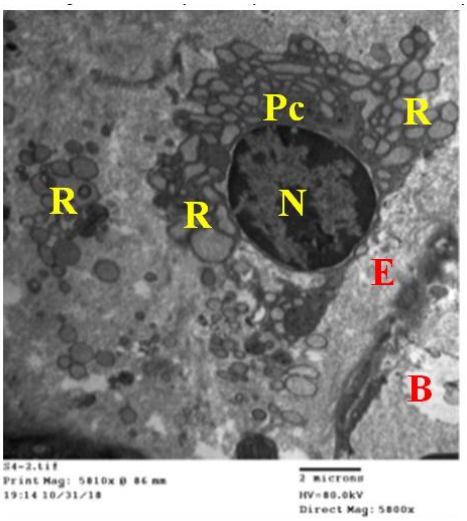


*Figure 18: T.E. micrograph of interstitial stroma of recovery group displayed: plasma cell (Pc) containing large amount of cystic dilated RER forming (Russel bodies) (R) and large vesicular nucleus (N) with peripheral clumping of chromatin, dilated blood vessel (B) and interstitial oedema (E) (TEM ×5800)*

## Discussion

Nucleotide inhibitors (NIs) have proved great promise as direct-acting antivirals; they have the

ability to produce potent and durable responses with broad genotypic coverage (Sofia, 2011) [26].

The exact mechanism behind SOF's effect may be attributed to the fact that SOF is a member of the NIs. Early generations of NIs were reported to cause toxicity, the mechanism for that could be attributed mainly to the fact that all HCV NIs are ribonucleotide analogues and therefore they had a great affinity for mitochondrial RNA polymerases than DNA polymerases. NIs that were incorporated by the mitochondrial RNA polymerase inhibited mitochondrial protein synthesis and showed a corresponding decrease in mitochondrial oxygen consumption in cells and this, in turn, leads to mitochondrial toxicity, cristolysis and cell death (Feng et al., 2016) [8].

The results of the present study proved that SOF administration resulted in time-dependent alterations in the SMSG. The alternations detected in the experimental subgroup (1) were serous acini swelling with vacuolated cytoplasm and accumulated intracellular secretory granules. GCTs and striated ducts revealed mild vacuolisation and eosinophilic retained secretion in the lumen. The gland presented with less compactness appearance duo to increase of oedema associated with intra-lobular fatty cellular infiltration.

These changes were aggravated in the subgroup (2) with detection of ghost-like masses of acini and ducts and extensive fatty cellular infiltration in the C.T. stroma. The parenchyma showed acinar and ductal shrinkage associated with less electron-dense secretory granules which were merged forming little lakes, severe vacuolisation, loss of most desmosomal junctions, dilatation of RER cisternae, cristolysis of the mitochondria and inflammatory cellular infiltration.

Regarding acinar Hypertrophy followed by shrinkage, (Salem et al., 2017) [21] concluded that the use of SOF for 60 days was accompanied by acinar and ductal shrinkage of the SMSG. (Dabrowska et al., 2006) [(4)] explained that as an adaptive mechanism and an attempt for glandular repair.

Extensive fatty cells infiltration detected in the present study was in agreement with (Salem et al., 2017) [21]; this fatty degeneration of the secretory portions was explained by (Scott, 1977) [23] as a characteristic finding of the aging process of salivary glands. Moreover, (Peluso, Villaño Valencia, Chen, & Palmery, 2018) [19] demonstrated that ROS generation was a key modulator of cell function and that oxidative status influences the pathophysiology of different tissues and could adversely affect tissues homeostasis and functioning as a signal mediator in inducing ageing of those tissues.

In consequence, ageing could be considered as another harmful effect of SOF, and this was in agreement with, (Issa and El-Sherif, 2017a) [12] who detected some ageing features in the cerebral cortex after SOF administration for 5 weeks.

Regarding inter and intra-lobular oedema, a similar finding was observed by (Issa and El-Sherif, 2017) [11] who confirmed the presence of focal areas of desquamation, separation and wide spaces of corneal epithelium indicating corneal oedema after SOF administration for 5 weeks. This histological finding was confirmed by our ultra-structural results inform of complete loss of intercellular junctions and widened of interstitial spaces.

Oedema occurs when an excessive volume of fluid accumulates in the tissues, which might compromise cellular metabolism in the swollen tissues and limit the diffusional removal of toxic byproducts of cellular metabolism (Scallan et al., 2010) [22].

The present study revealed the decrease in the fibrous C.T. thickness. This was similar to that demonstrated by (Issa and El-Sherif, 2017b) [11] who found wide separation and disarrangement to the collagen fibres bundles in addition to up-regulation of fibronectin expression in the retina of SOF treated rats. In an attempt to explain this, (El-Sisi and Zakaria, 2019) [7] concluded that SOF had an anti-fibrotic effect resulting in decrease collagen fibres organisation.

Regarding blood vessels congestion, extravasation of RBCs and mononuclear cellular infiltration, these were in one line with (Issa and El-Sherif, 2017a) [12] who showed vascular dilatation and extravasation of cerebral cortex blood vessels after SOF administration for 5 weeks. These findings could be considered as a part of the inflammatory process according to (Mubarak, 2012) [18] who stated that intolerable inflammation might lead to a microcirculatory disturbance with complete loss of capillaries integrity leading to hemorrhage which might have a role in SMSG degeneration.

In the present study vacuolar degeneration has affected the parenchyma of SMSG, such finding was in agreement with those of (Dyson et al., 2016 [5]; El Gharabawy et al., 2019 [6]). Vacuolar degeneration might be interpreted by the findings of (Lipshutz et al., 1995) [16] who attributed it to the damage of the mitochondria that were very vulnerable to noxious agents and when damaged, the cellular metabolism was failed, and sodium ions would enter the cell. This osmotic effect caused the breakdown of large macromolecules within the damaged cell leading to the appearance of cytoplasmic vacuoles. Our E.M. micrographs frequently presented mitochondrial affection.

The present study revealed ill-defined cell boundaries which were confirmed ultra-structurally and were in agreement with (Issa and El-Sherif, 2017b) [11] results after SOF administration for 5 weeks they found disruption of corneal cell membrane and fissures in the retina of the eye. This was explained by (Beneš et al., 1999) [3] who reported that

lipid peroxidation (LPO) was one of the main manifestations of oxidative stresses tissue damage leading to oxidative destruction of cell membranes.

In concern to striated duct loss of basal striation associating with severe affection of mitochondria, similar findings were mentioned by (Abdalla et al., 2017) [1] who confirmed the mitochondrial affection after SOF administration for 12 weeks. These results were explained by (Starkov and Wallace, 2002) [28] who attributed the mitochondrial changes of striated ducts to oxidative stresses.

In concern to GCTs, the histological picture showed congested tubules associated with coagulum stagnation. This was explained by (Lipshutz et al., 1995) [16] as the mitochondrial affection led to the depletion of (ATP) and failure of membrane pumps with subsequent no energy for secretion resulting in stagnant secretion.

Regarding the deterioration of SMSG parenchyma after 3 months of SOF administration, SOF was found to produce similar aggravated structural and ultrastructural changes in many organs. Rat visual cerebral cortex was an example, (Issa and El-Sherif, 2017a) [12] found that most neurons were distorted with vacuolated apoptotic cells and ghost-like masses after SOF treatment for 5 weeks. Regarding inflammatory cells infiltration, our results come in agreement with (Dyson et al., 2016) [5] who reported two cases treated with SOF and showed severe hepatitis C cirrhosis associated with acute parenchymal cellular infiltration and significant changes in many parameters. In contrast, (Teegen et al., 2019) [30] found a significant improvement of inflammation, fat content and fibrosis of liver transplant patients after SOF treatment for 12 weeks.

These alterations of SMSG were considered as a sign of toxicity according to (Balaban et al., 2005) [2] who attributed these changes to cell damage duo to mitochondrial toxicity and over-accumulation of reactive oxygen species (ROS).

Mitochondria play an important role in the generation of (ROS), which are produced physiologically during oxidative phosphorylation. Oxidative stresses occur if there is an imbalance between the production of (ROS) and cellular antioxidant defences. Oxidative stresses resulted in altered protein synthesis, disturbance of metabolism, organelles degeneration and even cell death by apoptosis (Tal et al., 2009) [29].

Amelioration of the induced structural changes in the recovery group was clearly shown; intralobular acini and duct system were more or less as a control group with mild vacuolisation. T.E. micrograph revealed numerous myoepithelial cells, different mitotic figures and inflammatory cells infiltration in the interstitial tissues, which had a great role in the immunological development. These were by (Kassab and Tawfik, 2018) [15] who found partial amelioration of SMSG in albino rats after the withdrawal of caffeinated energy drink.

In an attempt to explain this (Mohamed SS, 2015 [17]; Holmberg and Hoffman, 2014 [10]) assumed that the proliferation activity indices elevated after injury 2 folds in the acinar cells, 4 folds in intercalated duct cells and 10 folds in the myoepithelial cells, these mononuclear cells had self-renewal ability and could undergo endomitosis to duplicate DNA content as an adaptive attempt to replenish the damaged cells.

In conclusion, the discussed findings proved that intake of SOF has the potential to cause alteration in SMSG structure and ultrastructure through mitochondrial toxicity with subsequent changes in the gland homeostasis, the SMSG was shown a partial recovery of the normal structure after SOF withdrawal.

## References


1. Abdalla DA, Elhadidy TA, Besheer T, Farag RE. Respiratory adverse effects of sofosbuvir-based regimens for treatment of chronic hepatitis C virus. Egyptian Journal of Chest Diseases and Tuberculosis. 2017; 66(2):363-367. https://doi.org/10.1016/j.ejcdt.2016.12.004

2. Balaban RS, Nemoto S, Finkel T. Mitochondria, oxidants, and aging. Cell. 2005; 120(4):483-495. https://doi.org/10.1016/j.cell.2005.02.001 PMid:15734681

3. Beneš L, Ďuračková Z, Ferenčik M. Chemistry, physiology and pathology of free radicals. Life sciences. 1999; 65(18-19):1865-1874. https://doi.org/10.1016/S0024-3205(99)00439-7

4. Dabrowska E, Szynaka B, Kulikowska-Karpińska, E. Ultrastructural study of the submandibular gland of the rat after 6-month exposure to cadmium and zinc in drinking water. Advances in medical sciences. 2006; 51:245-249.

5. Dyson JK, Hutchinson J, Harrison L, Rotimi O, Tiniakos D, Foster GR, Aldersley MA, McPherson S. Liver toxicity associated with sofosbuvir, an NS5A inhibitor and ribavirin use. Journal of hepatology. 2016; 64(1):234-238. https://doi.org/10.1016/j.jhep.2015.07.041 PMid:26325535

6. El Gharabawy GSH, Abdallah EEA, Kaabo HF, Aleem A, Ahmed AM. Histological Effects of Sofosbuvir on The Kidney of Male Albino Rats and The Possible Protective Role of Vitamin C. The Egyptian Journal of Hospital Medicine. 2019; 76(1):3335-3354.

7. El-Sisi AE, Zakaria S. Potential Anti-Fibrotic Effect of Direct Acting Antiviral Drugs on CCl4 Induced Hepatic Fibrosis in Rats. Egyptian Journal of Basic and Clinical Pharmacology. 2019; 9. https://doi.org/10.32527/2019/101414

8. Feng JY, Xu Y, Barauskas O, Perry JK, Ahmadyar S, Stepan G, Yu H, Babusis D, Park Y, McCutcheon K. Role of mitochondrial RNA polymerase in the toxicity of nucleotide inhibitors of hepatitis C virus. Antimicrobial agents and chemotherapy. 2016; 60(2):806-817. https://doi.org/10.1128/AAC.01922-15 PMid:26596942 PMCid:PMC4750701

9. Fish R, Danneman PJ, Brown M, Karas A, editors. Anesthesia and analgesia in laboratory animals. Academic press; 2011.

10. Holmberg KV, Hoffman MP. Anatomy, biogenesis and regeneration of salivary glands. Vol. 24, Saliva: Secretion and Functions: Karger Publishers, 2014:1-13. https://doi.org/10.1159/000358776 PMid:24862590

PMCid:PMC4048853

11. Issa N, El-Sherif N. Histological and Immunohistochemical Studies on the Cornea and Retina of Sofosbuvir Treated Rats. Austin J Anat. 2017b; 4(2):1068. https://doi.org/10.26420/austinjanat.2017.1068

12. Issa N, El-Sherif N. Light and electronic histological studies to the effect of Sofosbuvir on the visual cerebral cortex of adult male albino rat. Journal of American Science. 2017a; 13(4):79-87.

13. 13. Jacobson IM, Gordon SC, Kowdley KV, Yoshida EM, Rodriguez-Torres M, Sulkowski MS, Shiffman ML, Lawitz E, Everson G.; Bennett, M. Sofosbuvir for hepatitis C genotype 2 or 3 in patients without treatment options. New England Journal of Medicine. 2013; 368(20):1867-1877. https://doi.org/10.1056/NEJMoa1214854 PMid:23607593

14. Johnson, A.A.; Ray, A.S.; Hanes, J.; Suo, Z.; Colacino, J.M.; Anderson, K.S.; Johnson, K.A. Toxicity of antiviral nucleoside analogs and the human mitochondrial DNA polymerase. Journal of Biological Chemistry. 2001; 276(44):40847-40857. https://doi.org/10.1074/jbc.M106743200 PMid:11526116

15. Kassab AA, Tawfik SM. Effect of a caffeinated energy drink and its withdrawal on the submandibular salivary gland of adult male albino rats: A histological and immunohistochemical study. Egyptian Journal of Histology. 2018; 41(1):11-26. https://doi.org/10.21608/EJH.2018.7518

16. Lipshutz BH, Stevens KL, Lowe RF. A novel route to the anti-HIV nucleoside d4T. Tetrahedron letters. 1995; 36(16):2711-2712. https://doi.org/10.1016/0040-4039(95)00374-L

17. Mohammed SS, El-Sakhawy MA, Sherif H, Shredah M. Effect of aspartame on submandibular salivary glands of adult male albino rats. Life Sci J. 2015; 12(3):44-50.

18. Mubarak R. Effect of red bull energy drink on rats submandibular salivary glands (light and electron microscopic study). J Am Sci. 2012; 8(1):366-72.

19. Peluso I, Villaño Valencia D, Chen CY, Palmery M. Antioxidant, Anti-Inflammatory, and Microbial-Modulating Activities of Nutraceuticals and Functional Foods 2018. Oxidative medicine and cellular longevity. 2018; 2018. https://doi.org/10.1155/2018/3824509 PMid:30116480 PMCid:PMC6079344

20. Ryan KJ, Ray CG. Medical microbiology. McGraw Hill. 2004; 4:370.

21. Salem ZA, Elbaz DA, Farag DB. Effect of an anti-hepatitis c viral drug on rat submandibular salivary gland. 2017.

22. Scallan J, Huxley VH, Korthuis RJ. Capillary fluid exchange: regulation, functions, and pathology. Colloquium Lectures on Integrated Systems Physiology-\nl\hspace* 18pt From Molecules to Function: Morgan & Claypool Publishers, 2010:1-94. https://doi.org/10.4199/C00006ED1V01Y201002ISP003

23. Scott J. A morphometric study of age changes in the histology of the ducts of human submandibular salivary glands. Archives of oral biology. 1977; 22(4):243-249. https://doi.org/10.1016/0003-9969(77)90109-1

24. Sene D, Ghillani-Dalbin P, Thibault V, Guis L, Musset L, Duhaut P, Poynard T, Piette JC, Cacoub P. Longterm course of mixed cryoglobulinemia in patients infected with hepatitis C virus. The Journal of rheumatology. 2004; 31(11):2199-2206. https://doi.org/10.1016/S0168-8278(04)90468-0

25. Shin JW, Seol IC, Son CG. Interpretation of animal dose and human equivalent dose for drug development. 2010; 31(3):1-7.

26. Sofia MJ. Nucleotide prodrugs for HCV therapy. Antiviral Chemistry and Chemotherapy. 2011; 22(1):23-49. https://doi.org/10.3851/IMP1797 PMid:21860070

27. Soriano V, Vispo E, de Mendoza C, Labarga P, Fernandez-Montero JV, Poveda E, Trevino A, Barreiro P. Hepatitis C therapy with HCV NS5B polymerase inhibitors. Expert opinion on pharmacotherapy. 2013; 14(9):1161-70. https://doi.org/10.1517/14656566.2013.795543 PMid:23621117

28. Starkov A, Wallace KB. Structural determinants of fluorochemical-induced mitochondrial dysfunction. Toxicological Sciences. 2002; 66(2):244-252. https://doi.org/10.1093/toxsci/66.2.244 PMid:11896291

29. Tal MC, Sasai M, Lee HK, Yordy B, Shadel GS, Iwasaki A. Absence of autophagy results in reactive oxygen species-dependent amplification of RLR signaling. Proceedings of the National Academy of Sciences. 2009; 106(8):2770-2775. https://doi.org/10.1073/pnas.0807694106 PMid:19196953 PMCid:PMC2650341

30. Teegen EM, Dürr M, Maurer MM, Eurich F, Vollbort A, Globke B, Bahra M, Blaeker H, Pratschke J, Eurich D. Evaluation of histological dynamics, kidney function and diabetes in liver transplant patients after antiviral treatment with direct-acting antivirals: Therapy of HCV-recurrence. Transplant Infectious Disease. 2019; 21(1):e13020. https://doi.org/10.1111/tid.13020 PMid:30375710

31. Thomas DL. Curing hepatitis C with pills: a step toward global control. Lancet. 2010; 376(9751):1441. https://doi.org/10.1016/S0140-6736(10)61497-3

32. Zeng QL, Zhang JY, Zhang Z, Wang LF, Wang FS. Sofosbuvir and ABT-450: terminator of hepatitis C virus? World journal of gastroenterology: WJG. 2013; 19(21):3199. https://doi.org/10.3748/wjg.v19.i21.3199 PMid:23745021 PMCid:PMC3671071